

Instrument Science Report ACS 2012-01

Flux Calibration of the ACS CCD Cameras

IV. Absolute Fluxes

Ralph C. Bohlin
February 6, 2012

ABSTRACT

ISRs I–III in this series define the charge transfer efficiency (CTE) for the CCD detectors, the encircled energy fractions, and the optical throughput degradation. This fourth ISR establishes the absolute flux calibration for the photometry, as corrected with the algorithms specified in I–III. Synthetic photometry from the SEDs of three primary hot 30,000–60,000K WDs define these sensitivity calibrations for the standard HRC and WFC filters. Even though the external uncertainty for the absolute flux of the three primary WD flux standards is $\sim 1\%$, the internal consistency of the sensitivities is $\sim 0.3\%$. However, when these WD sensitivities are applied to the cooler F, G, and K stars, there are internal inconsistencies of 1–2% for the F775W, F814W, and F850LP filters. For the same cooler stars, the other broadband filters are internally consistent to better than the 1% ACS flux calibration goal after applying the corrections and calibrations specified here. One filter F435W requires a small shift of the long wavelength edge of the bandpass by 18\AA toward longer wavelengths in order to reduce the cool star residuals from as much as 2% to $< 0.5\%$; but wavelength shifts cannot remedy the flux discrepancies for the F, G, and K stars in the three long wavelength filters.

For HRC, the sensitivities change by 0.5–2% as a monotonic function of wavelength because of improvements in data processing. Additional residual corrections for individual filters are typically $< 0.5\%$ for wide filters in both cameras. For the medium and narrow filters, these residuals are as large as $\sim 3\%$ for the WFC F550M and $\sim 4\%$ for HRC F344N. After implementing these throughput updates, the synthetic predictions of the WFC and HRC count rates for the average of the three primary WD standard stars agree with the observations to 0.1% for every filter.

1. Introduction

The calibration of the ACS filter complement is based on the observations of spectrophotometric standards and the application of synthetic photometry techniques (De Marchi et al. 2004, DeM; Sirianni et al. 2005, S05, Bohlin 2007a, B07). The transmission of the filters, the throughput of the optics, and the quantum efficiency of the detectors are measured in the lab and combined to form a total system throughput. The essence of the ACS absolute flux calibration is the comparison of fully corrected observed count rates, C , in electrons/s for flux standards with the predicted count rates, P , from the integral of the product of the stellar flux and the total throughput for each filter. The first three ISRs in this series dealt with the required corrections: I. the CTE correction (Bohlin & Anderson 2011), II. the encircled energy (EE) correction (Bohlin 2011, ISR-II), and III. the correction for the loss of sensitivity with time (Bohlin, Mack, & Ubeda 2011, ISR-III). Deviations of the corrected observed count rates from the predictions of the synthetic photometry are corrected by DeM, S05, and B07 by adjusting the detector QE and the filter transmission. This work updates the QE results found by B07 and specifies the required adjustments to the filter transmissions. S05 and references therein provide details of the instrumental design and a summary of the pipeline data processing.

Table 1 of ISR-II lists the number of standard star observations with ACS photometry in the two CCD cameras, WFC and HRC. In addition, there are new WFC observations of P330E on 2011 July 14. The observed count rates are measured with the standard one arcsec radius of S05 and with an additional new standard 0.5'' radius to aid the common case of crowded star fields where no star is isolated enough for reliable 1.0'' photometry. §2 documents the encircled energy corrections for the new 0.5'' standard radius, which supplements the EE for the 1.0'' radius. EE for apertures that are much less than 0.5'' (10 WFC pixels) is less repeatable because of the variability of the HST PSF. For the best accuracy with small aperture photometry, each individual ACS image should be analyzed to define the EE of the small aperture relative to either the standard 1.0 or 0.5'' aperture. Because the 1.0'' photometry is slightly more repeatable than the newly defined 0.5'' case, the fully corrected 1.0'' photometry divided by the EE is used in this work as the measure of the count rate in the “infinite” 5.5'' radius of S05. Additional corrections for the CTE losses of Bohlin & Anderson (2011) and for the changing sensitivity with time (ISR-III) are applied along with the sensitivity change for lower WFC CCD temperature on side 2 (Mack et al. 2007).

Section 3 makes the case for a small wavelength shift of the F435W filter. The final HST WD based flux calibration is presented in §4, which details the wavelength dependent

corrections to the CCD QEs and the additional multiplicative factors required to update the filter transmissions. The new reference files are documented in §5, while the final §6 is a mini user’s guide for flux calibration.

2. Encircled Energy Corrections for 0.5" Radius

ISR-II derived the EE in a 1" aperture, which is required to establish the flux calibration of the ACS according to the methodology of S05. However, many science images are too crowded or too noisy for accurate photometry in such a large aperture. Thus, the EE for a smaller 0.5" radius is more useful to a larger science community; and the 0.5" EE at the WFC1-1K reference point on CCD chip-1 is tabulated here for each filter following the derivation in ISR-II for the EE in a 1" aperture. Average EE values in a 0.5" radius for the ten bright standard stars are displayed in Figures 1 and 2 as a function of the filter pivot wavelength. The analysis is the same as detailed in ISR-II, and Table 1 summarizes the results from the fitted curves. Typical formal 1σ uncertainties on the fitted values in Table 1 are 0.005 for WFC and 0.008 for HRC, which compare with the similar uncertainties for the 1" EE from ISR-II of 0.003 and 0.007. Photometric uncertainties in single GO images are usually much larger than uncertainties in either the 0.5 or the 1.0" mean correction of EE to infinite aperture. Thus, the 0.5" reference aperture is as precise for most measurements of absolute flux as the 1.0" adopted in this ISR. Table 1 also includes the results for the EE in the 1.0" aperture, where a few values differ from ISR-II by 0.001 because of the new data.

The new EE values are within 1–2% of the corresponding S05 results. For example, the biggest difference with S05 for the WFC EE in a one arcsec aperture is 0.009 for F475W, which now has 13 measures at WFC1-1K with a 3σ rms of only 0.006. Even though S05 is a well established refereed reference for EE and for the flux calibration, the new values are more reliable because of the much larger set of measurements and because many of the S05 calibration data are subarray observations with no overscan. Because of the extreme sensitivity of the photometry in the 5.5" infinite aperture to background subtraction, the current analysis requires the overscan pixels that are needed for precise removal of the CCD bias level. The switch to the WFC1-1K subarrays with overscan began in 2003 with programs 10054, PI Giavalisco and 10056, PI Gilliland, so that a few standard star observations from the early results of S05 are still included in the current analysis, which utilizes only the WFC1-1K subarray centered at (3584,1536). The corresponding S05 EE measures at the WFC1 and WFC2 reference points at (2100,1024) are consistent with the new results for WFC1-1K but show larger scatter. For example in F475W, the EE for observations of GRW+70°5824 have ranges of 0.920–0.947 and 0.934–0.960 for five EE measures at each of

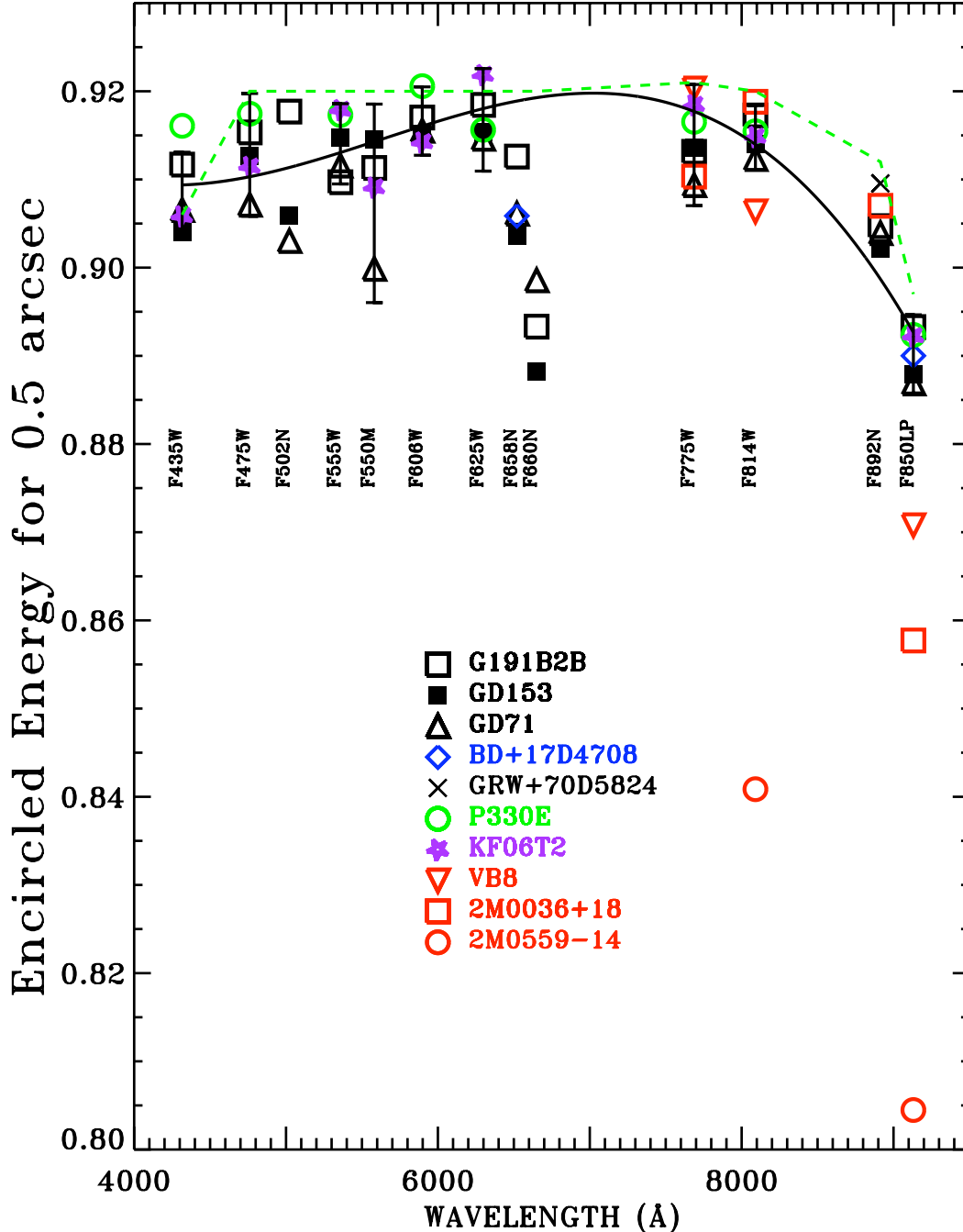


Fig. 1.— Encircled energy for WFC, i.e. fraction of signal in a 0.5 arcsec aperture relative to an “infinite” aperture of 5.5 arcsec radius. The solid black line is a cubic fit to only the broadband filter EE means for the WDs, the F star (BD+17°4708), the G star (P330E), and the K star (KF06T2). Error bars for the filters used for the polynomial fit are $\pm 3\sigma$ error in the mean of these averages, but the averages are not shown to avoid crowding. The green dashed lines are the corresponding results of S05.

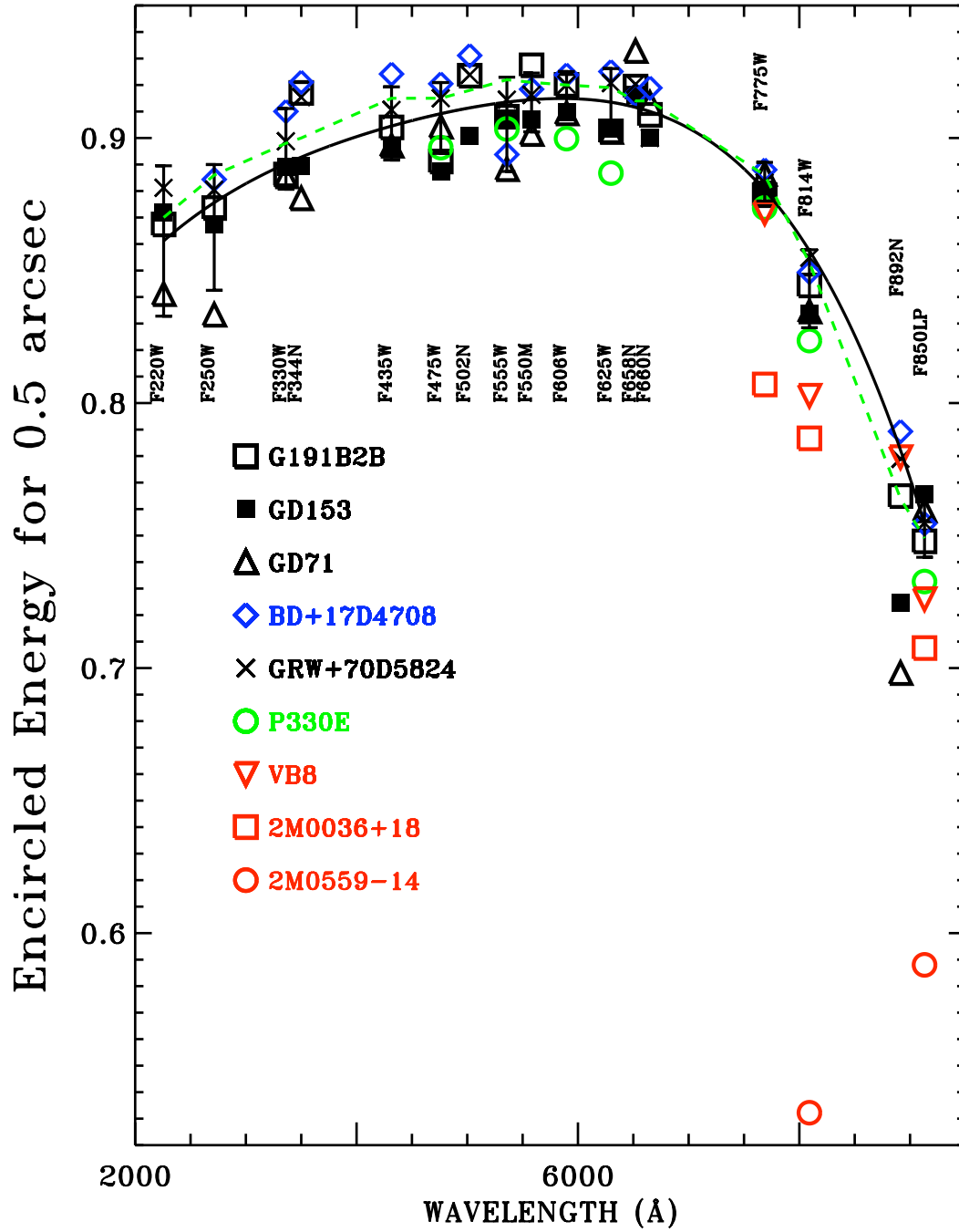


Fig. 2.— As in Figure 1 for HRC, except that there are no data for the K star (KF06T2) and the polynomial fit is quartic.

WFC1 and WFC2, respectively. These ranges are both much larger than for the WFC1-1K data but do encompass the adopted value of 0.943 from Table 1. The S05 data without overscan are of lower fidelity but do suggest that any variation of the EE correction around the field of view is less than 1% for photometry with large radii on the order of one arcsec.

Red stars of spectral type M and later have a “red halo” and show significantly lower EE, because long wavelength photons scatter more in the CCD substrates, especially for HRC, which lacks the special anti-scattering layer incorporated into the WFC CCDs. Figures 1 and 2 show these red star EE values as red data points. S05 provide their tables 6-7, which define the EE vs. effective wavelength. These effective wavelengths are not constant for a filter but increase as the peak of the stellar flux distributions move to longer wavelengths. While ISR-II tabulated the EE for red stars in 1'' apertures, Table 2 has the corresponding results for 0.5'' photometry. S05 fits the early EE results as a function of effective wavelength, but the new values in Table 2 are derived directly from the measurements. Both WFC visits to the reddest star, 2M0559-14 (T6.5), are at the WFC1-1K reference point, even the one observation that was analyzed by S05.

| Filter | WFC(0.5'') | HRC(0.5'') | WFC(1.0'') | HRC(1.0'') |
|--------|------------|------------|------------|------------|
| F220W | ... | 0.861 | ... | 0.940 |
| F250W | ... | 0.876 | ... | 0.937 |
| F330W | ... | 0.890 | ... | 0.936 |
| F344N | ... | 0.893 | ... | 0.936 |
| F435W | 0.909 | 0.905 | 0.942 | 0.938 |
| F475W | 0.910 | 0.909 | 0.943 | 0.940 |
| F502N | 0.911 | 0.911 | 0.944 | 0.942 |
| F555W | 0.913 | 0.914 | 0.945 | 0.943 |
| F550M | 0.914 | 0.914 | 0.946 | 0.944 |
| F606W | 0.916 | 0.915 | 0.947 | 0.945 |
| F625W | 0.918 | 0.914 | 0.948 | 0.945 |
| F658N | 0.919 | 0.912 | 0.949 | 0.944 |
| F660N | 0.919 | 0.910 | 0.950 | 0.943 |
| F775W | 0.918 | 0.880 | 0.950 | 0.923 |
| F814W | 0.914 | 0.857 | 0.948 | 0.906 |
| F892N | 0.899 | 0.782 | 0.942 | 0.851 |
| F850LP | 0.893 | 0.754 | 0.939 | 0.830 |

Table 1: *Encircled Energy Fractions for K type and hotter stars in 0.5'' and 1.0'' apertures.*

| Filter | Hot-Star | VB8 (M7) | | 2M0036(L3.5) | | 2M0559(T6.5) | |
|------------|----------|----------|-------|--------------|-------|--------------|-------|
| | | New | S05 | New | S05 | New | S05 |
| (1) | (2) | (3) | (4) | (5) | (6) | (7) | (8) |
| WFC | | | | | | | |
| F814W | 0.914 | 0.91 | 0.92 | 0.92 | 0.91 | 0.84* | 0.90 |
| F892N | 0.899 | ... | 0.90 | 0.91 | 0.90 | ... | 0.90 |
| F850LP | 0.893 | 0.87* | 0.87 | 0.86* | 0.85 | 0.80* | 0.78 |
| HRC | | | | | | | |
| F775W | 0.880 | 0.87 | 0.87* | 0.81 | 0.86* | ... | 0.85* |
| F814W | 0.857 | 0.80 | 0.79* | 0.79 | 0.78* | 0.53 | 0.75* |
| F892N | 0.782 | 0.78 | 0.77* | ... | 0.77* | ... | 0.77* |
| F850LP | 0.754 | 0.73 | 0.69* | 0.71 | 0.67* | 0.59 | 0.55* |

Table 2: *Encircled Energy for 0.5'' for very cool stars. Use column (2) values, which are from Table 1, except for the values that are flagged with an asterisk. Compare with table 3 of ISR-II for EE in 1''.*

The sparse EE measures for red stars often have low count rates, so that the EE values have larger uncertainties than the 1σ values 0.005 for WFC and 0.008 for HRC quoted above for the ensemble hotter-star values in Table 1 that are copied to column two of Table 2. Table 2 contains the recommended values of the EE for later type stars of M (VB8), L (2M0036+18), and T (2M0559-14) for the long wavelength filters, where the Table 1 EE values are not appropriate. Only VB8 in the three longwave broadband filters has count rates above the cutoff limits for the hotter stars, i.e. 16,000 electrons/s for WFC and 10,000 electrons/s for HRC. For WFC, the only discrepancy with S05 is for 2M0559-14 in the F814W filter. There are two direct measures of this 0.5'' EE, 0.827 and 0.852, both of which are below the S05 value of 0.90 and both of which are at the WFC1-1K reference point. Part of this difference is that S05 had only the WFC1-1K 2003 data set that corresponds to the EE of 0.852, but this point is absent from the S05 figure 9, despite the fact that the F850LP value at WFC1-1K for 2M0559-14 is included. Probably, most of the difference is because the S05 value of 0.90 in their table 6 is from their figure 9 of EE values vs. effective wavelength, which omits the F814W point for 2M0559-14. However, the difference of 0.06 between the new value and S05 is probably comparable to the uncertainty in either set of results. Similarly, the two EE values for 2M0559-14 in the F850LP are 0.790 and 0.817. Because of the additional observations not available to S05, the directly measured values for WFC in F814W for 2M0559-14 and for all three red stars in F850LP in Table 2 are recommended, whereas the Table 1

values are adopted for all other WFC cases. Because only a few HRC observations with poor S/N are available, all of the smoothly parameterized EE of S05 in Table 2 are adopted (see ISR-II) and flagged with an asterisk. For example, the most discrepant 2M0559-14 value of 0.53 for F814W is from a single observation with a formal uncertainty of 0.3. The Table 1 HRC values are recommended for SEDs similar to the cool star types M, L, or T in filters shortward of F775W.

In summary, for flux distributions similar to the red curves in figure 3 of ISR-II, the EE for hotter stars is not appropriate for estimating the mean flux in the longer wavelength filters. Differences with the S05 results are due to a more robust set of observations and the inclusion of all of the data in the analysis.

3. Shift of the F435W Bandpass

In the case of the F435W filter, the comparison of the observed count rates in electrons/s, C, of the flux standards with the predicted count rates, P, shows an anomalous trend with stellar temperature as shown in the lower panel of Figure 3. The observed count rates in comparison to the synthetic photometry show a systematic increase with cooler stellar temperatures. The K1.5III star KF06T2 is discrepant by $2\% \pm 0.2\%$, i.e. 10σ . The two independent measures of KF06T2 with F435W agree to 0.3%, and both of pairs of WFC photometry for BD+17°4708 (sdF8) and P330E (G0V) agree to 0.1%. The trend in the lower panel of Figure 3 suggests a problem with the currently specified filter bandpass.

The lab measurements of the bandpass of F435W before flight show that the transmission varies with position on the filter. In particular, the long wavelength cutoff has a total range of variation of 52\AA among the four measured positions, while the short wavelength edge has a scatter of only 10\AA (D. Golimowski private comm.) Thus, the main cause of the WFC discrepancy in the lower panel of Figure 3 is likely caused by a deviation from the F435W average laboratory transmission at the long wavelength edge; and a 18\AA shift toward longer wavelengths of the long wavelength portion of the filter bandpass function raises the P values of the cooler stars with respect to P for the hot WDs. Such a shift for WFC reconciles the discrepant measurements of the various stellar types and is a likely and straightforward solution to a securely measured photometric inconsistency. In the top panel of Figure 3 after correcting the F435W bandpass function, all of the WD observations are within 1% of their new average; and most of the photometry, C, is within 0.5% of the synthetic prediction, P. While the newly determined bandpass function may not be the same at other positions on the filter, at least there is a determination of the throughput for one position, i.e. the WFC1-1K reference point. In order to be assured of achieving the ACS flux

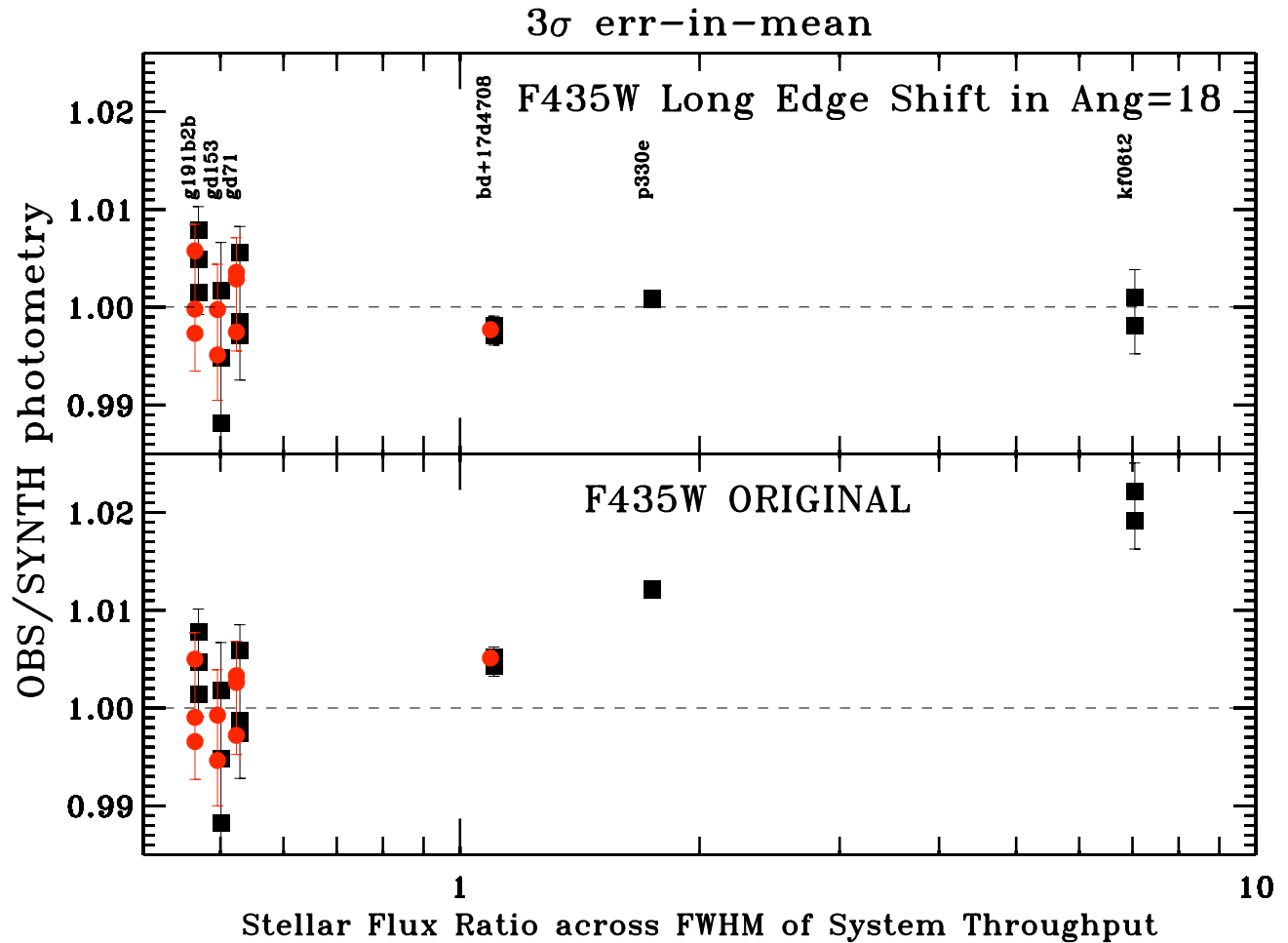


Fig. 3.— F435W photometry for the primary standard WDs and three cooler stars shown as a function of the ratio of the stellar flux across the F435W bandpass from 3900 to 4800Å. Black squares are WFC data, while red circles are HRC. In the lower panel for the current F435W bandpass function, the cooler stars are systematically too bright in comparison to the synthetic photometric predictions. In the top panel, the discrepancy for the WCF disappears when the long wavelength edge of the filter bandpass is shifted by 18Å toward longer wavelengths.

calibration accuracy goal of 1%, the science target should be placed at this same WFC1-1K position, where the filter bandpass has been determined.

For HRC, the 18Å shift does not improve the the solitary BD+17°4708 point; and thus, no shift of the HRC bandpass is proposed.

Unfortunately, there are no observations of any of the F, G, or K stars at other locations on the detector to assess the general applicability of the shifted F435W bandpass found at the WFC1-1K reference point. The K star KF06T2 provides the most sensitive test of the long wavelength cutoff of F435W; and a set of ~ 12 subarrays with overscan could be obtained in one orbit to test the new WFC transmission curve over an equally spaced grid. Single observations do not test repeatability, but precision is maximized by collecting as many photons as possible in every calibration orbit without saturating the stellar images. Each standard star exposure records around a million electrons to achieve a typical statistical precision of 0.1%.

4. Traditional Calibration on the HST WD Flux Scale

The majority of the S05 flux calibration data were of the secondary standard GRW+70°5824, while a few observations of the primary standard GD71 were also considered. However, the secondary standard GRW+70°5824 has only one STIS observation at 3065–5450Å and two in the 5450–10000Å range. The additional uncertainty is $\sim 1\%$ in the assignment of the GRW+70°5824 absolute flux relative to the three primary WD standards. Beginning with B07, the ACS flux calibration is derived directly on the HST flux scale, which is based on the three primary standards GD153, GD71, and G191B2B. These three SEDs are defined by pure hydrogen model atmosphere calculations (eg. Bohlin et al. 2011).

As a reference example for ACS photometry, Tables 3–4 include the stellar coordinates in pixels within the WFC1-1K subarray, the exposure times, and the photometry of prime standards in 0.5 and 1" apertures for one visit with each camera. The photometry and sky level are in electrons s^{-1} from the `_crj` ACS pipeline data product and are corrected with the pixel area maps (PAMs) for each camera. The sky is measured in the annulus from radius 6–8" for WFC and from 5.6–6.5" for HRC, as in S05.

4.1 Sensitivity Variations around the WFC Field

The ACS flux calibration program has a modest goal of obtaining the best understanding of sensitivities near one reference point in each of the HRC and WFC cameras. The accuracy

| Filter | x(px) | y(px) | exp (s) | 0.5'' | 1'' | sky (e/s) |
|--------|--------|--------|---------|----------|----------|-----------|
| F435W | 497.8 | 514.5 | 4.0 | 147859.2 | 153311.6 | 0.053 |
| F475W | 497.7 | 514.9 | 3.0 | 189452.7 | 196220.2 | 0.103 |
| F502N | 497.3 | 514.9 | 90.0 | 5433.2 | 5622.9 | -0.000 |
| F550M | 497.6 | 515.2 | 10.0 | 48401.9 | 50216.7 | -0.011 |
| F555W | 497.6 | 514.6 | 4.6 | 114023.1 | 117942.1 | 0.073 |
| F606W | 497.4 | 514.6 | 2.6 | 201719.0 | 208733.0 | 0.221 |
| F625W | 497.4 | 514.9 | 5.0 | 102064.2 | 105772.8 | 0.084 |
| F658N | 497.9 | 515.2 | 120.0 | 4555.2 | 4736.5 | 0.008 |
| F660N | 498.0 | 514.5 | 300.0 | 1779.7 | 1876.7 | 0.001 |
| F775W | 497.4 | 514.7 | 9.0 | 57182.5 | 59295.6 | 0.044 |
| F814W | 497.9 | 514.5 | 8.0 | 69300.7 | 71870.7 | 0.096 |
| F850L | 497.6 | 515.1 | 24.0 | 20056.3 | 21082.7 | 0.026 |
| F892N | 1009.2 | 1025.0 | 220.0 | 2139.0 | 2220.7 | 0.008 |

Table 3: *Sample WFC photometry in electrons s^{-1} in 0.5'' and 1'' apertures for GD71 obtained in a one orbit visit at 2003.84 on 2003 Nov 3. The values are from the j8v602*_crj files processed 2011 May 11 and corrected by the PAMs. The F892N data are centered in the full 2048x2048 quadrant B, rather than in the WFC1-1K subarray utilized for the other filters.*

of these sensitivities at other positions on the CCD chips is determined by the precision of the flat fields, which are monitored by other programs such as earth flats and by the internal flats (Bohlin et al. 2005; Gilliland, Bohlin, & Mack 2006; Gilliland & Bohlin 2007). The current ACS CCD L-flats have an estimated accuracy of $\sim 1\%$ (Mack et al. 2002); but stepping a bright standard star around the chips would verify and quantify the precision obtained by these flat fields without the stellar crowding that complicates similar goals in the 47 Tuc calibration program. To supplement the orbit proposed above for KF06T2 and F435W, a WD should be stepped at the same F435W positions. Similarly, the WFC field-of-view (FOV) should be explored in the same way for the important long wavelength filter F850LP, using a WD and an IR bright star. Depending on results from such a four orbit pilot program, the spacial dependence of the sensitivity for hot vs. cool stars could be explored for additional, heavily-used filters.

The HST/ACS archive contains one case of a star stepped around the WFC FOV as illustrated in Figure 4. Except for one point on the edge of CCD 2, the response at the other seven widely spaced locations is uniform to $\pm 0.5\%$. Such uniformity is surprisingly good, as

| Filter | x(px) | y(px) | exp (s) | 0.5'' | 1'' | sky (e/s) |
|--------|-------|-------|---------|----------|----------|-----------|
| F220W | 498.2 | 514.5 | 4.0 | 196114.9 | 213950.0 | 0.105 |
| F250W | 498.3 | 514.2 | 5.0 | 177578.9 | 191254.0 | 0.003 |
| F330W | 498.4 | 514.2 | 4.0 | 171192.3 | 179915.4 | 0.050 |
| F344N | 498.3 | 514.4 | 60.0 | 15831.2 | 16573.2 | 0.006 |
| F435W | 498.3 | 514.7 | 4.0 | 295604.9 | 305809.9 | 0.024 |
| F475W | 498.8 | 514.3 | 3.0 | 379027.5 | 392485.6 | -0.006 |
| F502N | 498.5 | 514.3 | 100.0 | 11155.3 | 11523.5 | -0.000 |
| F550M | 498.7 | 514.4 | 14.0 | 103326.1 | 106733.0 | 0.010 |
| F555W | 498.7 | 514.0 | 6.0 | 236854.1 | 244394.3 | 0.047 |
| F606W | 498.4 | 514.1 | 3.0 | 402128.1 | 415932.4 | -0.013 |
| F625W | 498.6 | 514.3 | 6.0 | 195744.5 | 202349.5 | 0.053 |
| F658N | 499.0 | 514.3 | 140.0 | 8982.5 | 9281.4 | 0.002 |
| F660N | 498.2 | 514.2 | 400.0 | 3468.0 | 3587.3 | -0.000 |
| F775W | 498.4 | 514.1 | 14.0 | 88935.4 | 93083.0 | 0.013 |
| F814W | 498.3 | 514.3 | 14.0 | 107039.6 | 113108.6 | 0.021 |
| F850L | 498.6 | 514.2 | 30.0 | 32911.5 | 36043.8 | 0.012 |
| F892N | 498.7 | 514.1 | 200.0 | 3384.6 | 3679.1 | 0.001 |

Table 4: *Sample HRC photometry (j8v603*_crj) in electrons s⁻¹ for G191B2B obtained in a one orbit visit at 2003.85 on 2003 Nov 8 and processed by the ACS pipeline on 2011 May 11.*

the F775W has a range of 72Å for the long wavelength cutoff, which is the largest scatter among the six measured filters (D. Golimowski private comm.)

Any offset between the WFC1-1K and S05 reference points at WFC1 and WFC2 are minimal, as shown in Figure 5, which illustrates the ratio of the ACS photometry at WFC1 (top panel) or WFC2 (bottom panel) to the average photometry at WFC1-1K for observations of the same star. Only primary WD stars (black squares) were observed at both WFC2 and WFC1-1K, where the broadband filters (filled black squares) show a slight tendency to fall above unity by a few tenths of a percent. The corresponding trend for the filled black squares for WFC1 is just the opposite, so that any actual difference between the sensitivities at WFC1-1K and the S05 average of WFC1+WFC2 is of order 0.1–0.2%. The larger scatter for the narrower band filters (open black squares) suggests variability around the FOV may be at the ~1% level rather than the <0.5% for the broadband filters.

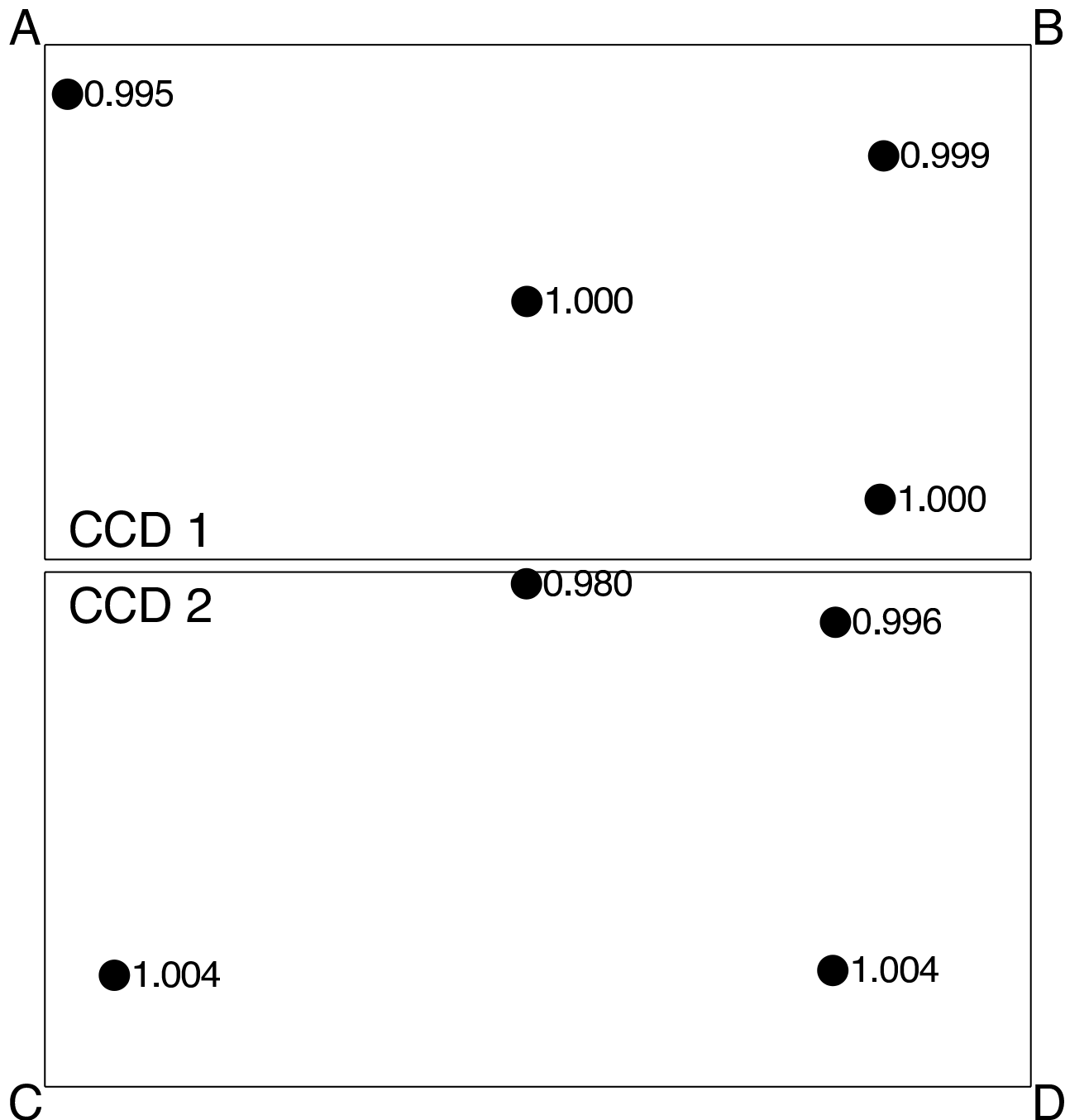


Fig. 4.— Relative response around the WFC FOV with F775W for observations of G191B2B on 2002 July 31 from program 9568. The 0.980 point at the top of CCD chip 2 is probably inaccurate because a large fraction of the sky background region lies off the CCD. Otherwise, the photometric response is uniform to $\pm 0.5\%$. The 0.999 point at the upper right of chip 1 is at the WFC1-1K reference point, while the 1.000 value near the center of chip 1 is near the WFC1 reference point.

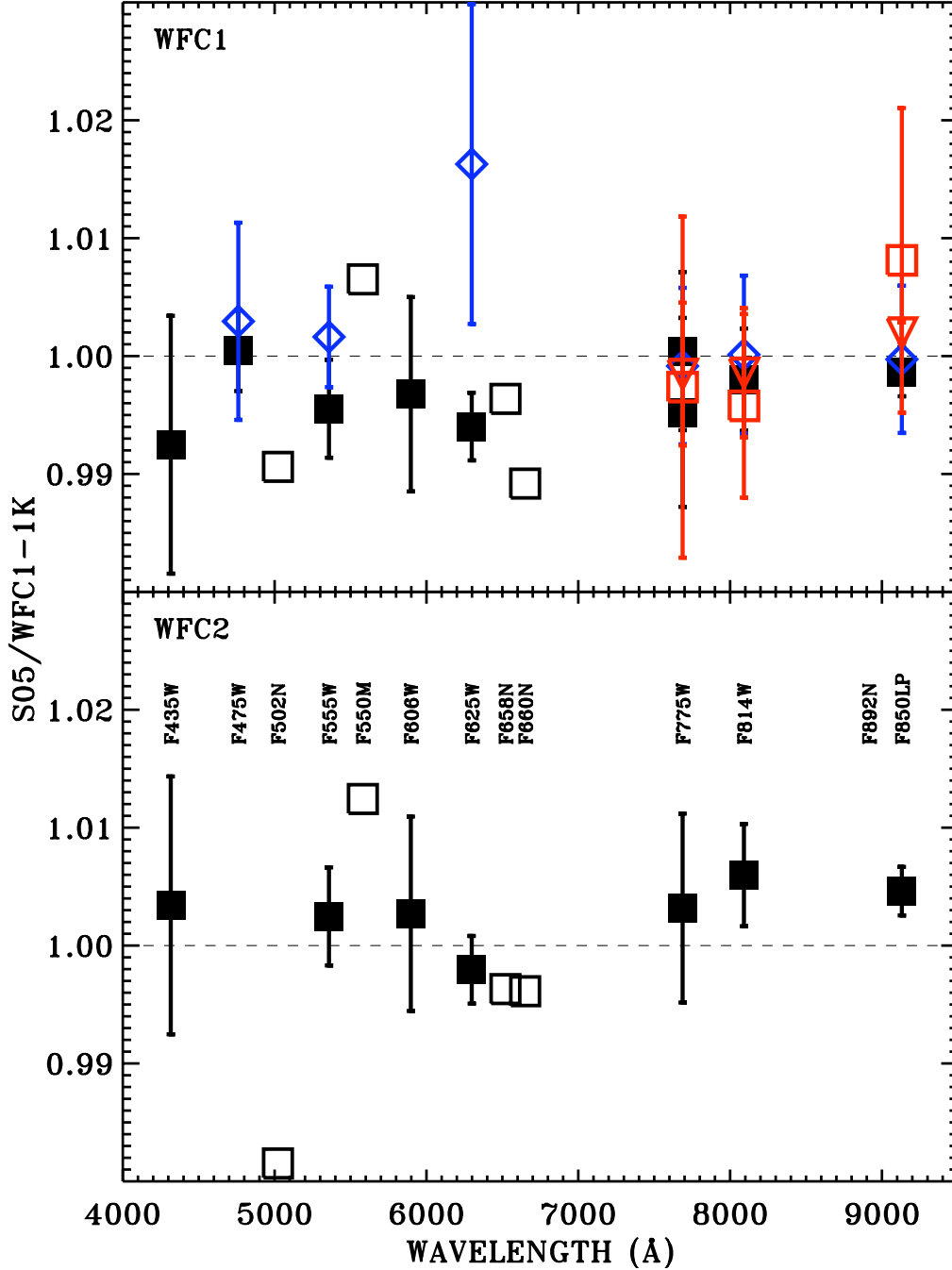


Fig. 5.— Response at the old S05 absolute flux reference points WFC1 (top) and WFC2 (bottom) relative to the current WFC1-1K absolute flux reference point. Black squares are the primary WD standard stars, G191B2B or GD71, where filled black is for the broadband filters and open black squares are narrow and medium bandpasses. Blue diamonds are BD+17°4708, while the red points are the red M and L stars as defined in Figure 1. Occasionally, the often saturated BD+17°4708 data has a larger scatter, because `_flt` files must be used instead of the more noise free `_crj` files.

4.2 Corrections for QE as a Function of Wavelength

In the remainder of this ISR, the standard WFC1-1K reference point at (3583,1535) on CCD chip 1 is used for WFC. These observations are restricted to be within 8.4 arcsec of the WFC1-1K subarray center in order to avoid flat field uncertainties and edge effects, while stars are restricted to be within 6.5 arcsec of chip center for HRC. HRC F220W and F250W have no on-orbit L-flats; and the flux errors could be of order 10% at other points in the field of view. Pedigrees for the standard star SEDs used to compute the predicted response, P in electrons/s, are documented elsewhere, eg. Bohlin et al. (2011), which also specifies the equations used to compute the P values. In order to measure the ACS response C in electrons/s, the pipeline `_crj` files are corrected with pixel area maps (PAMs) and used as input to the *IDL* photometry routine *apphot* (Landsman, private comm.), where the pixel with peak signal is always less than the respective WFC and HRC saturation levels of $\sim 80,000$ and $\sim 140,000$ electrons in each image of the CR-split pair. After correction by the PAMs, the `_crj` data are equivalent to `_drz` photometry. For BD+17°4708 with WFC, the `_flt` files are used because of saturation caused by the minimum reliable exposure time of two seconds. Gilliland (2004) demonstrated the excellent linearity of ACS for saturated data, where excess charge just bleeds along the columns and is not lost. However, cosmic ray rejection routines (i.e. `_crj` files) are not appropriate for heavily saturated data; and the bleeding must be less than the radius of the photometry aperture.

After correcting the 1" photometry C values for the EE, the CTE losses, the loss of sensitivity with time, and the F435W filter shift, the ACS C/P values for the WD stars appear in Figures 6–7 for WFC and HRC, respectively. (Neither the tiny CTE losses for the 1" photometry per Bohlin & Anderson (2011) nor the small sensitivity losses from ISR-III are included in the Table 3–4 values.) In Figures 6–7, squares are averages for the three prime WDs as shown with their 3σ error in the mean, while the red crosses for the secondary WD standard GRW+70°5824 demonstrate good agreement. Following DeM and B07, the broadband filters (filled squares) are fit, ignoring the more deviant medium and narrow band filters (open squares). The linear fits correct the QE as a function of wavelength, while the remaining residuals define errors in average filter transmission. Values for F220W and F250W may need revision after on-orbit L-flats are produced.

Except for F435W with synthetic photometry P from the newly shifted bandpass, the broadband filters in Figure 6 are consistent with an average level of unity for C/P. However for HRC in Figure 7, the fit shows significant changes from the QE of B07. The main cause of these changes is an improved algorithm for computing the bias levels. In Figure 7, the coefficients for the linear HRC fit as a function of wavelength are 1.0238 and -2.08×10^{-6} .

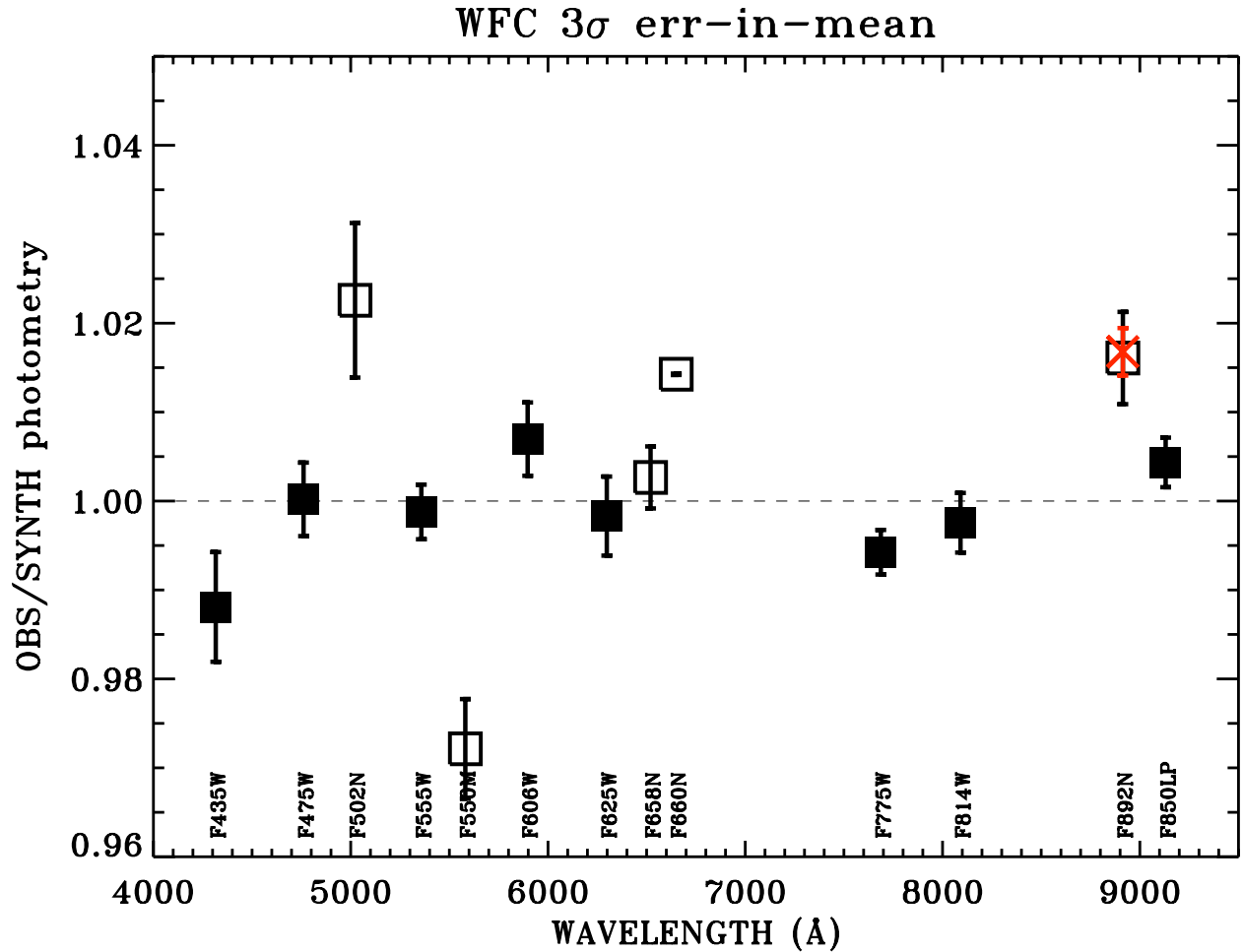


Fig. 6.— Fully corrected C/P count rate ratios vs. pivot wavelength for the WD stars observed with WFC. Squares are averages of the three prime WDs G191B2B, GD153, and GD71 with their 3σ errors in the mean, while the red X represents the slightly cooler GRW+70°5824. Except for F435W, the broadband filters (filled squares) are consistent with an average of unity. B07 showed more GRW+70°5824 data points; however, most of those observations are early in the ACS life and used different reference points.

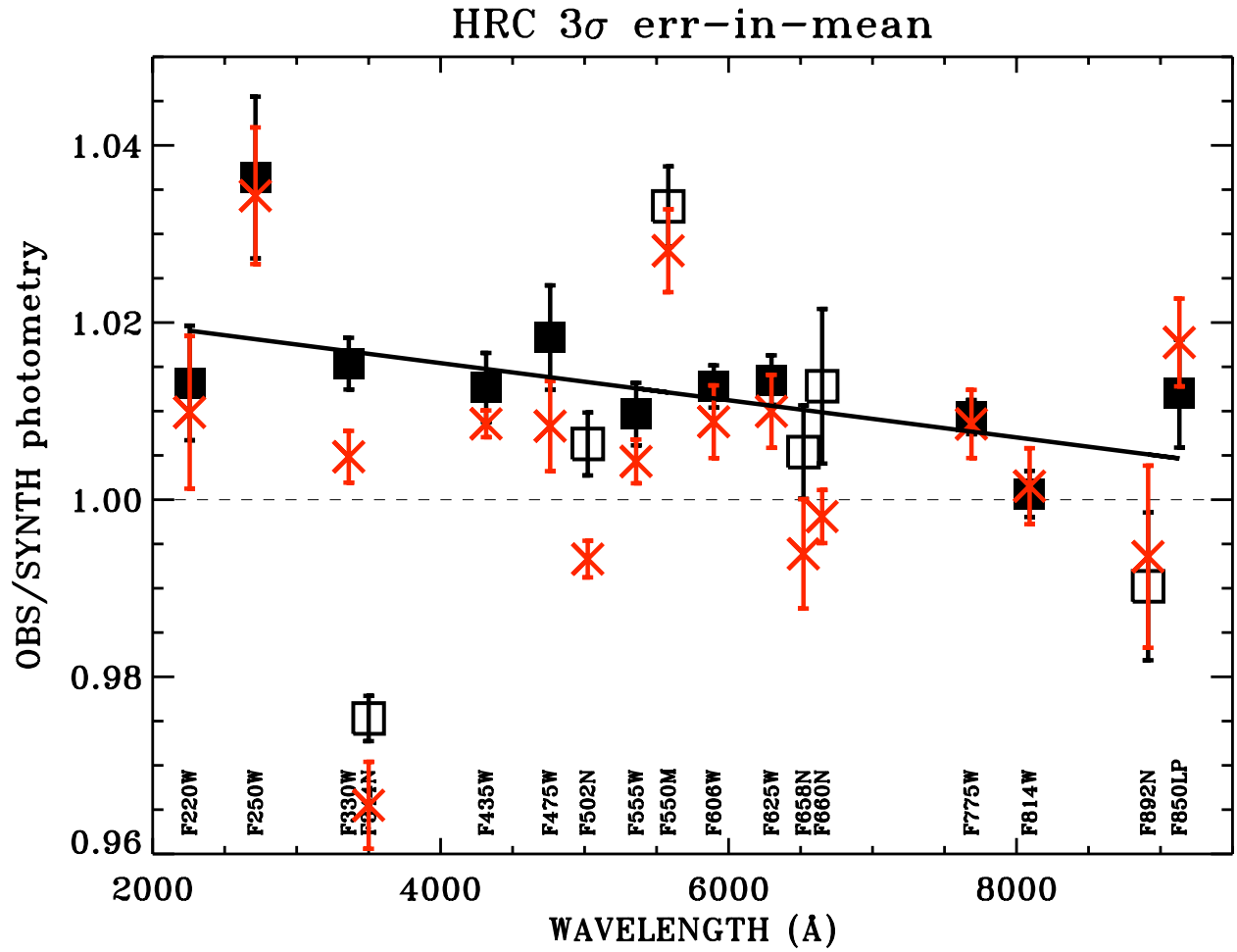


Fig. 7.— As in Figure 6 for HRC. Following DeM, a smooth linear fit (heavy line) to the broadband filters (filled squares) is made, ignoring the more deviant medium and narrow band filters (open squares).

4.3 Adjustments for Individual Filters

The differences between the average point (square) for each filter and unity for Figure 6 and between the linear fit (heavy line) and the squares in Figure 7 define the required corrections to the filter transmissions. These residual corrections need not be the same for WFC and HRC, because the stellar light rays strike at different positions on the physical filter and because the WFC and HRC flat fields are normalized arbitrarily and not to each other. Table 5 includes the linear fit values in the columns labeled “QE change” and required residual corrections with their uncertainties in the columns labeled “Filter Residuals”.

| Filter | QE-Change | | Filter-Residual | | | |
|--------|-----------|-------|-----------------|-----------|-------|-----------|
| | WFC | HRC | WFC | 3σ | HRC | 3σ |
| F220W | ... | 1.019 | ... | ... | 0.994 | 0.006 |
| F250W | ... | 1.018 | ... | ... | 1.018 | 0.009 |
| F330W | ... | 1.017 | ... | ... | 0.999 | 0.003 |
| F344N | ... | 1.017 | ... | ... | 0.960 | 0.002 |
| F435W | 1.000 | 1.015 | 0.988 | 0.006 | 0.998 | 0.004 |
| F475W | 1.000 | 1.014 | 1.000 | 0.004 | 1.004 | 0.006 |
| F502N | 1.000 | 1.013 | 1.023 | 0.009 | 0.993 | 0.003 |
| F550M | 1.000 | 1.012 | 0.972 | 0.006 | 1.021 | 0.004 |
| F555W | 1.000 | 1.013 | 0.999 | 0.003 | 0.997 | 0.003 |
| F606W | 1.000 | 1.012 | 1.007 | 0.004 | 1.001 | 0.002 |
| F625W | 1.000 | 1.011 | 0.998 | 0.004 | 1.003 | 0.003 |
| F658N | 1.000 | 1.010 | 1.003 | 0.004 | 0.995 | 0.005 |
| F660N | 1.000 | 1.010 | 1.014 | 0.000 | 1.003 | 0.009 |
| F775W | 1.000 | 1.008 | 0.994 | 0.003 | 1.002 | 0.002 |
| F814W | 1.000 | 1.007 | 0.998 | 0.003 | 0.994 | 0.003 |
| F850LP | 1.000 | 1.005 | 1.004 | 0.003 | 1.007 | 0.006 |
| F892N | 1.000 | 1.005 | 1.016 | 0.005 | 0.985 | 0.008 |

Table 5: *QE and Filter Transmission Updates. The 3σ uncertainties of the residuals are errors-in-the-mean.*

The HST software package *Synphot* has been recently converted to use the Python software code and renamed *Pysynphot*. Results from the two packages are equivalent, except for the PHOTBW keyword values, so that the two names are used synonymously herein. Pysynphot utilizes the instrumental QE, the filter transmissions, and the optical throughput curves vs. wavelength to calculate the instrumental flux calibrations listed in the *fits* headers

for every HST observation. Traditionally, the average of the two cameras has been used to update the Synphot filter component throughput, because the same physical filter is used for both. However, the WFC/HRC differences are sometimes greater than the 3σ uncertainties, notably for F550M; and therefore, Synphot must differentiate between WFC and HRC filter transmission curves.

A verification of the typical uncertainties in the filter corrections is the average absolute difference of 0.5% between the red crosses and filled squares for the 11 broadband HRC filters in Figure 7. Larger differences for the narrow band filters can be caused by noise in the minimal STIS observations of the standard star spectrum of GRW+70°5824 or by the finite resolution at $H\alpha$ that would affect the predicted count rate P for F658N and F660N. Model SEDs are used for the three prime WDs; and the development of a high fidelity model SED for GRW+70°5824 could alleviate these two deficiencies.

4.4 After Iteration

After making the corrections for the side 2 temperatures, the EE, the changes with time, the CTE, the F435W filter shift for WFC, the QE, and the filter transmissions, the average photometry for the three prime WDs is corrected to exactly agree with the average synthetic photometry from their pure hydrogen model SEDs as shown in Figures 8–9. The fully corrected broadband photometry for the F, G, and K stars in Figures 8–9 is within 1% of agreement, except for the longer wavelength filters, as discussed in the next section, and except for three HRC UV filters. This 1% scatter for ACS observation of the cooler star with respect to the WDs includes the uncertainties in the Table 5 corrections and is indicative of the consistency of the STIS flux calibration relative to ACS. No added systematic uncertainty accrues from the EE correction of Tables 1–2 when photometry is referenced to a one arcsec radius, which is the same choice made here for defining the throughput corrections. Of course in the final analysis, errors in individual science images are often dominated by noise, crowding, or lack of repeatability for small radius photometry.

The HRC UV filters have only sparse observations of BD+17°4708 for comparison with the WDs. The STIS CALSPEC¹ reference spectrum is dropping rapidly in flux from the F330W bandpass toward the F220W range. However, there is no reason to doubt the validity of the SED, as all three STIS G230LB spectra agree to 0.2% with their mean, even in the shortest band with 66,870 photo-electrons in the 2000–2400Å range. The most likely causes for the 2–3% residuals for F220W, F250W, and F330W are errors in the out-of-band

¹<http://www.stsci.edu/hst/observatory/cdbs/calspec.html>

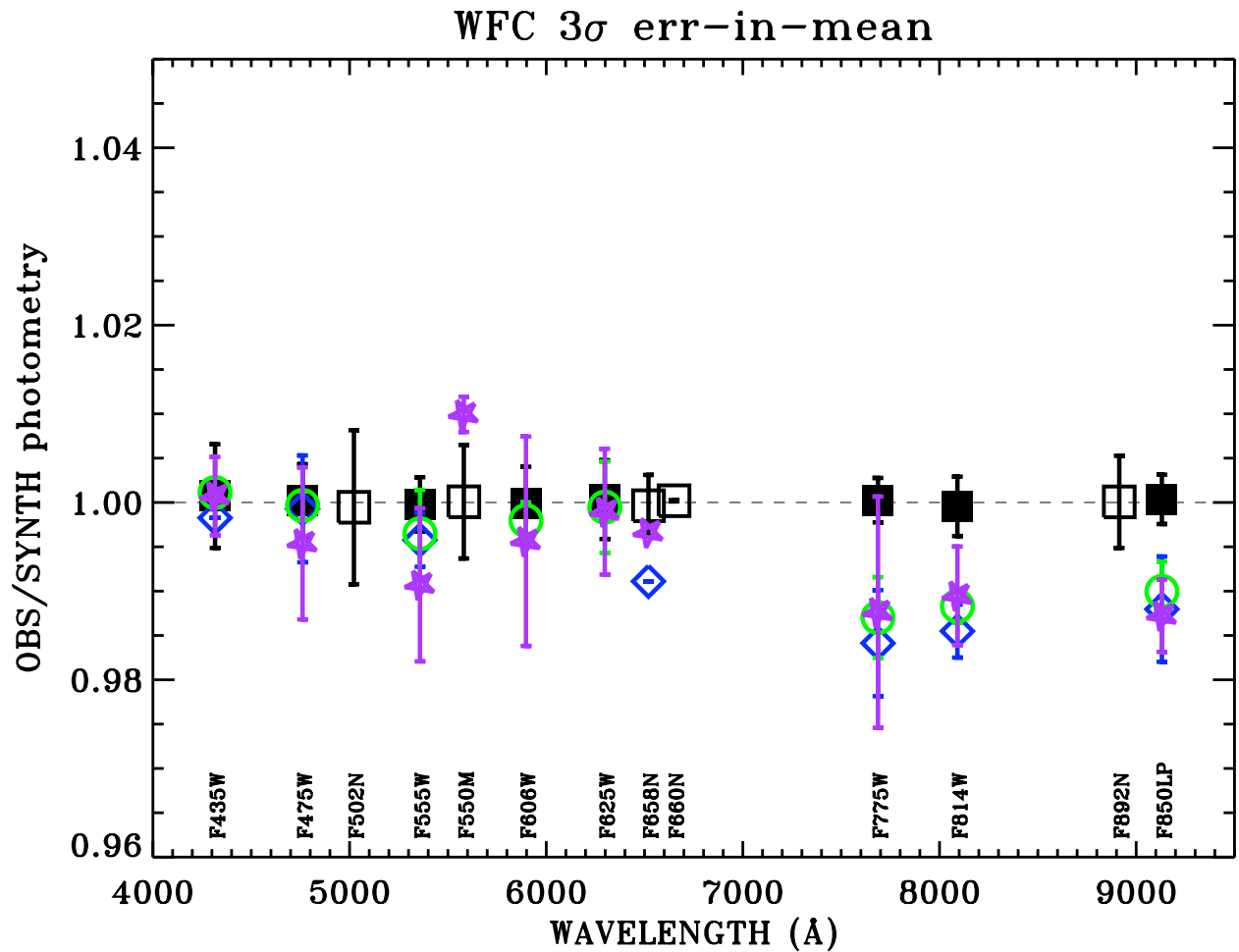


Fig. 8.— C/P count rate ratios vs. pivot wavelength for the stars observed with WFC, as in Figure 6, but after making the corrections for the F435W filter shift and the corrections in Table 5 for the QE and filter transmission. The black squares for the average of the three prime WDs are now all within 0.001 of unity, while the averages and 3σ error-in-the-mean are shown for the F (blue diamond), G (green circle), and K (purple star) standards.

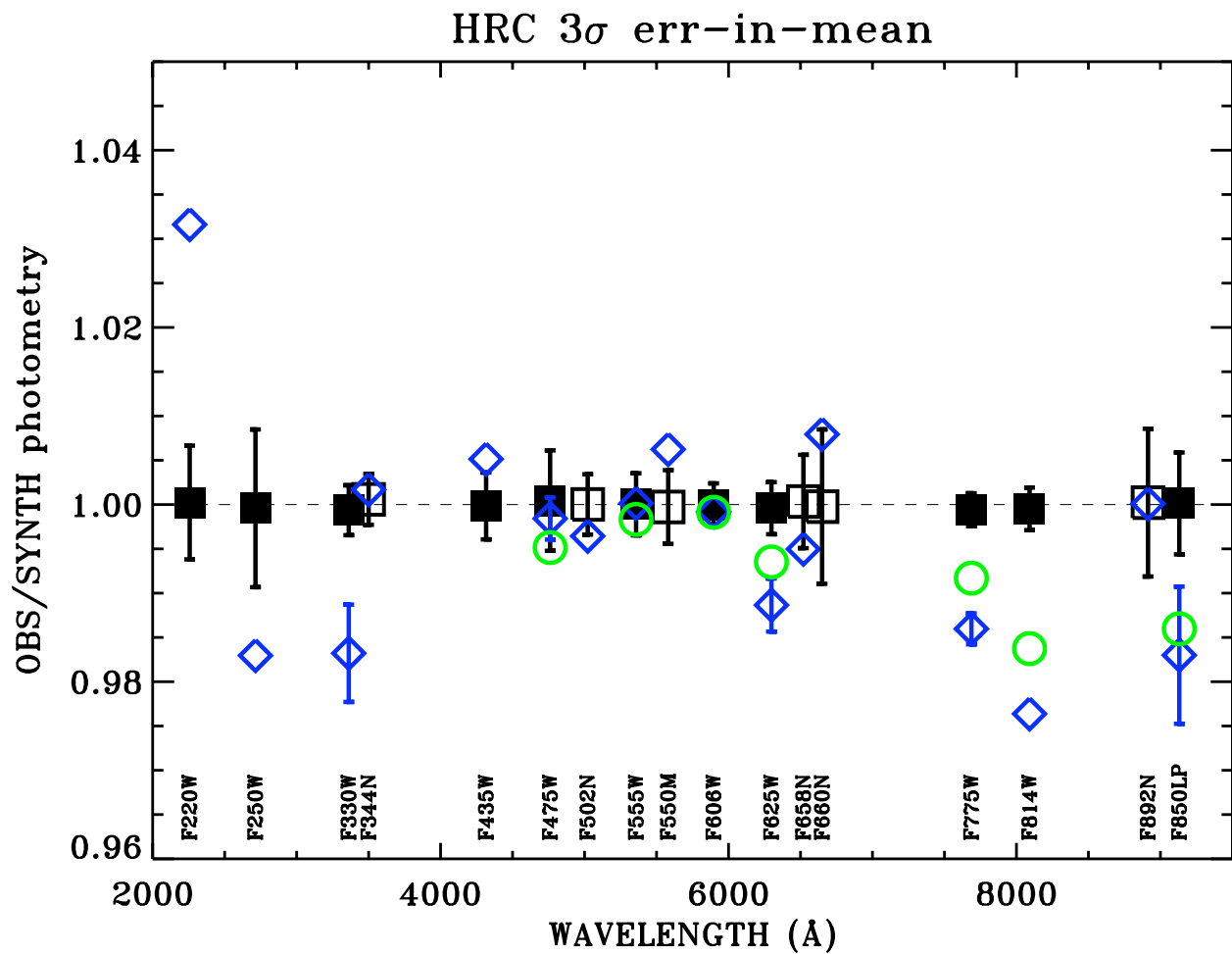


Fig. 9.— As in Figure 8 for HRC, except that there are no observations of the new K1.5III flux standard, KF06T2.

transmission measures or small wavelength shifts of the filter at the reference point, as found above for F435W. Because of the lack of confirming HRC observations of G or K type standards, no filter shifts are proposed for these three UV filters.

4.5 Long Wavelength Inconsistencies

The three long wavelength broadband filters, F775W, F814W, and F850LP show residuals that are generally greater than 1% in Figures 8–9. For example, all three filters deviate from unity for WFC in Figure 8 by more than 10σ for the well measured G type star, P330E. B07 explored various explanations for these discrepancies and dismissed several possible causes, such as errors in the STIS background subtraction, scattered light from the STIS gratings, ACS non-linearity, ACS filter red light leaks, ACS QE errors, and ACS filter shifts. In addition, STIS CTE errors can be eliminated as a problem, because the F type star, BD+17°4708 is so much brighter than the three primary WDs, P330E, and KF06T2. The main effect of any STIS CTE correction error would be to change the flux of BD+17°4708 with respect to the G and K stars; however, the F, G, and K stars all have similar C/P values for the three problematic filters.

One other possibility is a filter blue leak that would raise the computed synthetic photometry P for the WDs with respect to the cooler stars that have little UV flux. However, to change the WD computed P values by 1%, the out-of-band transmissions would need to rise from the measured $\sim 10^{-6}$ longward of 4000Å to $\sim 10^{-3}$; or a leak bigger than 1% in the unmeasured 3000–4000Å region would be required. Thus, the cool star photometric error in the three long wavelength broadband filters remains a mystery; and the uncertainty in that photometry is $\sim 2\%$, rather than the goal of 1%, which is achieved for the five broad filters from F435W to F625W.

5. New Pipeline Reference Files

5.1 QE Curves

The Synphot QE reference files for the WFC and HRC CCD detectors are structured with wavelength in column 1, a default QE in column 2 for unspecified dates, and then pairs of QE columns, where the actual QE at any date is linearly interpolated in time between the dates for columns 3 and 4, columns 5–6, etc. This scheme is reflected in Table 7, as discussed in the next section. For example in the case of HRC, there is only one pair of QE columns with dates of 2002.16 and the end of HRC operations at 2007.1 (MJD=54136).

For WFC, the QE changed at 2006.5 with the switch to the side 2 electronics chain when the operating temperature was lowered, so that the first pair of QE columns 3–4 for -77C cover the date range 2002.16–2006.5 (MJD 52334–53919), while the second pair for -81C is currently for 2006.5–2021.0 (MJD 53920–59214). However, during SM4 in 2009 May, the ACS WFC electronics repair changed the conversion from analog CCD output in ADU to electrons, which is equivalent to a new QE starting at 2009.4. Thus, the second pair of columns (5–6) will now cover the time range 2006.5–2009.4 (MJD 53920–54976), while a new pair (7–8) will cover 2009.4–2021.0 (MJD 54977–59214). The ACS CCD channels were inactive from early 2007 until after the SM4 servicing mission at 2009.4, i.e. a MJD of 54977; but no harm is done by defining a correction during this dead time.

Currently, there is no correction to *photflam* in the ACS data headers for the gradually changing sensitivity specified in ISR-III of this series; and to implement this correction, each column of the current pairs must be multiplied by the wavelength dependent relative sensitivity of ISR-III for the reference date associated with each column. In particular for WFC, column 3 for the initial epoch 2002.16 has no correction to the B07 values, column 4 is column 3 multiplied by the time correction for 2006.5, column 5 is the original column 5 for -81C, corrected by the same 2006.5 time change vector, and column 6 is the original column 5 corrected to 2009.39. ISR-III provided a fourth order polynomial fit to the linear loss rates in %/year over the time period 2002.2–2007.1. The coefficients for the wavelength dependence of the fit are -0.03180, 2.035e-05, -5.184e-09, 5.652e-13, and -2.189e-17, which differ slightly from ISR-III because of the new P330E observation. After SM4 in 2009, there are insufficient data to define a trend with time, so that the columns 7–8 of the new WFC QE file are both the same product of the original column 5 and the time correction for 2009.41, where this correction is defined by a cubic fit in wavelength with coefficients 1.210, -9.644e-05, 1.372e-08, and -6.077e-13.

In addition to the time dependent changes, the time independent QE updates of §4.2 are incorporated by multiplying every QE column in the reference files by the WFC or HRC linear fits to those QE updates. The WFC fit is set to unity, which retains the B07 QE determination for the initial epoch at 2002.16. The new QE file names are `acs_wfc_ccd2_mjd_021_syn.fits` and `acs_hrc_ccd_mjd_015_syn.fits`.

5.2 Filter Transmissions

Updated filter curves are created by adjusting for the multiplicative constants in the Filter-Residual columns of Table 5 and by the +18Å shift of the long wavelength edge of F435W with WFC. Because the corrections for WFC and HRC differ, there are now two

filter curves that replace each single file that served to compute ACS CCD sensitivities in the past. The version of the newly delivered filter throughputs are listed in Table 6.

| Filter Transmission File Name |
|-------------------------------|
| acs_f435w_wfc_006_syn.fits |
| acs_f475w_wfc_006_syn.fits |
| acs_f502n_wfc_007_syn.fits |
| acs_f550m_wfc_007_syn.fits |
| acs_f555w_wfc_005_syn.fits |
| acs_f606w_wfc_007_syn.fits |
| acs_f625w_wfc_006_syn.fits |
| acs_f658n_wfc_007_syn.fits |
| acs_f660n_wfc_007_syn.fits |
| acs_f775w_wfc_005_syn.fits |
| acs_f814w_wfc_006_syn.fits |
| acs_f850lp_wfc_006_syn.fits |
| acs_f892n_wfc_007_syn.fits |
| |
| acs_f220w_hrc_007_syn.fits |
| acs_f250w_hrc_005_syn.fits |
| acs_f330w_hrc_007_syn.fits |
| acs_f344n_hrc_006_syn.fits |
| acs_f435w_hrc_006_syn.fits |
| acs_f475w_hrc_006_syn.fits |
| acs_f502n_hrc_007_syn.fits |
| acs_f550m_hrc_007_syn.fits |
| acs_f555w_hrc_005_syn.fits |
| acs_f606w_hrc_007_syn.fits |
| acs_f625w_hrc_006_syn.fits |
| acs_f658n_hrc_007_syn.fits |
| acs_f660n_hrc_007_syn.fits |
| acs_f775w_hrc_005_syn.fits |
| acs_f814w_hrc_006_syn.fits |
| cs_f850lp_hrc_006_syn.fits |
| acs_f892n_hrc_007_syn.fits |

Table 6: *Names of the Updated Filter Transmission Files.*

6. Absolute Fluxes, Magnitudes, and Zero-Points

The effective flux for photometry is defined as an integral over wavelength range λ of the filter bandpass

$$\langle F_\lambda \rangle = \frac{\int F_\lambda \lambda R d\lambda}{\int \lambda R d\lambda} = P_\lambda N_e , \quad (1)$$

where F_λ is the stellar flux distribution (SED), R is the instrumental system throughput, P_λ is the calibration constant *photflam* that appears in the HST data headers, and N_e is the stellar signal in electrons per second ($e s^{-1}$) for infinite aperture photometry (Bohlin et al. 2011). The notation P_λ should not be confused with P used above for the predicted count rates, while N_e can be either the observed (C) or predicted (P) in $e s^{-1}$. Values for the source independent P_λ are calculated from the product of the component throughputs, i.e. total system throughput R and the collecting area A of the primary mirror, where h is Planck's constant, c is the speed of light, and the integral is over the wavelength range of the filter.

$$P_\lambda = \frac{hc}{A \int \lambda R d\lambda} \quad (2)$$

Because of the change in ACS sensitivity with time as implemented in the new QE files described above in §5.1, *photflam*, i.e. P_λ , changes with time. The *photflam* appropriate to the time of observation should appear in the data header keyword *PHOTFLAM* for each ACS observation. Table 7 includes sample *photflam* values for the dates of the columns in the QE reference files.

Because the measurement of N_e in an “infinite” 5.5” aperture is impractical for most science images, a smaller reference aperture radius $r = 0.5$ or $1.0''$ should be used with the EE from Table 1 (or from Table 2 for the coolest stars).

$$N_e = \frac{N_e(r)}{EE(r)} , \quad (3)$$

so that

$$\langle F_\lambda \rangle = P_\lambda \frac{N_e(r)}{EE(r)} \quad (4)$$

Photometry for smaller apertures suffers from the variability of the HST PSF, so that the EE corrections for each individual ACS image must be referenced to an isolated star using a 0.5 or 1.0” radius.

Many astronomers prefer magnitudes to fluxes for measures of stellar brightness. The standard definition of a magnitude scale is

$$m = -2.5 \log(F/F_o) = -2.5 \log(F) + 2.5 \log(F_o) = -2.5 \log(F) + C , \quad (5)$$

| Filter | WFC | | | | | HRC | |
|--------|-----------------|----------------|----------------|----------------|----------------|-----------|-----------|
| | MJD52334 | MJD53919 | MJD53920 | MJD54976 | MJD54977 | MJD52334 | MJD54136 |
| | 2002.16 -77C | 2006.5 -77C | 2006.5 -81C | 2009.4 -81C | 2009.4 -81C | 2002.16 | 2007.1 |
| F220W | | | | | | 7.969e-18 | 8.226e-18 |
| F250W | | | | | | 4.589e-18 | 4.697e-18 |
| F330W | | | | | | 2.191e-18 | 2.227e-18 |
| F344N | | | | | | 2.182e-17 | 2.217e-17 |
| F435W | 3.076e-19 | 3.113e-19 | 3.187e-19 | 3.213e-19 | 3.149e-19 | 5.275e-19 | 5.347e-19 |
| F475W | 1.786e-19 | 1.807e-19 | 1.842e-19 | 1.857e-19 | 1.827e-19 | 2.872e-19 | 2.911e-19 |
| F502N | 5.136e-18 | 5.197e-18 | 5.286e-18 | 5.328e-18 | 5.252e-18 | 7.953e-18 | 8.060e-18 |
| F550M | 3.906e-19 | 3.952e-19 | 4.005e-19 | 4.037e-19 | 3.984e-19 | 5.768e-19 | 5.845e-19 |
| F555W | 1.928e-19 | 1.950e-19 | 1.979e-19 | 1.995e-19 | 1.968e-19 | 2.979e-19 | 3.019e-19 |
| F606W | 7.712e-20 | 7.797e-20 | 7.893e-20 | 7.951e-20 | 7.844e-20 | 1.258e-19 | 1.274e-19 |
| F625W | 1.175e-19 | 1.188e-19 | 1.201e-19 | 1.209e-19 | 1.193e-19 | 1.940e-19 | 1.964e-19 |
| F658N | 1.954e-18 | 1.974e-18 | 1.994e-18 | 2.008e-18 | 1.981e-18 | 3.330e-18 | 3.370e-18 |
| F660N | 5.169e-18 | 5.222e-18 | 5.275e-18 | 5.312e-18 | 5.240e-18 | 8.842e-18 | 8.946e-18 |
| F775W | 9.904e-20 | 9.962e-20 | 1.009e-19 | 1.013e-19 | 9.994e-20 | 1.928e-19 | 1.941e-19 |
| F814W | 6.939e-20 | 6.968e-20 | 7.077e-20 | 7.096e-20 | 7.007e-20 | 1.268e-19 | 1.274e-19 |
| F850LP | 1.501e-19 | 1.503e-19 | 1.538e-19 | 1.539e-19 | 1.521e-19 | 2.263e-19 | 2.265e-19 |
| F892N | 1.484e-18 | 1.485e-18 | 1.516e-18 | 1.517e-18 | 1.500e-18 | 2.472e-18 | 2.475e-18 |

Table 7: ACS infinite aperture calibration constants *photflam*, i.e. P_λ in units of $erg\ s^{-1}\ cm^{-2}\ \text{\AA}^{-1}/(e\ s^{-1})$. The applicable dates are listed as MJD and as fractional year, along with the WFC CCD set point temperature. The P_λ at any date is the linear interpolation between pairs of columns, except that P_λ is constant at the values in the fifth WFC column after 2009.4=MJD54977.

where F_o is a reference flux and C is constant called a zero point. Common zero points are -21.1 for the ST magnitude system, or -48.6 for the AB mag (Smith et al. 2002) system, where F is in frequency units of $erg\ s^{-1}\ cm^{-2}\ Hz^{-1}$, rather than the $erg\ s^{-1}\ cm^{-2}\ \text{\AA}^{-1}$ units used for the ST mag system.

Another popular system is Vega magnitude, where F_o is the flux of Vega, which can be found in the CALSPEC² archive. However, Vega is an HST secondary standard; and

²<http://www.stsci.edu/hst/observatory/cdbs/calspec.html>

its CALSPEC flux is from STIS spectrophotometry, which is based on the three primary WD standards (Bohlin & Gilliland 2004, Bohlin 2007b). The best estimate for the Vega flux changes whenever better STIS calibrations are derived. For example, an improved STIS gain ratio (Goudfrooij et al. 2009) resulted in a change of the V band mag from 0.026 to 0.031. If the goal is precise ratios of the flux of an object at different wavelengths, as required for SNIa SEDs used in the study of dark energy, the slope of the STIS SED relative to the primary WD SEDs can change, for example whenever the wavelength dependent correction for STIS sensitivity losses or CTE is updated. For the best precision in multi-wavelength flux ratios of HST data, use the calibrated fluxes directly, because HST flux calibrations are based on the three primary WD standard candles, not Vega.

For data calibrated directly with respect to contemporaneous Vega observations, as often done for ground based observations, the conversion to fluxes via the CALSPEC SED of Vega is not correct at the longer wavelengths because a model is used that omits the actual extra emission from Vega's dust ring. For example using interferometric techniques, Absil. et al. (2006) measured a 1.29% contribution from the dust ring for a wavelength as short as 2.1 μm .

Finally, instrumental magnitudes m_I are often quoted (S05). For example substituting in Equation 5 for ST magnitudes

$$m = -2.5\log(P_\lambda N_e) - 21.1 = -2.5\log(P_\lambda) - 2.5\log(N_e) - 21.1 = m_I - 2.5\log(P_\lambda) - 21.1, \quad (6)$$

where m_I is $-2.5\log(N_e)$ and $N_e = N_e(r)/EE(r)$. The instrumental magnitude zero points for $N_e = 1$ are easily calculated from Table 7 as $-2.5\log(P_\lambda) - 21.1$.

Acknowledgement

Thanks to Adam Riess for suggesting the inclusion of Tables 3–4 and the discussion of magnitude systems. Matt McMaster performed extensive testing of the new reference files before delivery; and David Golimowski provided the results of the F435W lab measurements along with many helpful comments on an early draft.

References

- Absil, O., et al. 2006, A&A, 452, 237
 Bohlin, R. C. 2007a, Instrument Science Report, ACS 2007-06, (Baltimore:STScI) (B07)

- Bohlin, R. C. 2007b, in ASP Conf. Ser. 364, The Future of Photometric, Spectrophotometric, and Polarimetric Standardization, ed. C. Sterken (Ann Arbor, MI: Sheridan Books), 315
- Bohlin, R. C. 2011, Instrument Science Report, ACS 2011-02, (Baltimore:STScI) (ISR-II)
- Bohlin, R. C., & Anderson, J. 2011, Instrument Science Report, ACS 2011-01, (Baltimore:STScI)
- Bohlin, R. C., & Gilliland, R. L. 2004, AJ, 127, 3508
- Bohlin, R. C., Mack, J., & Ubeda, L. 2011, Instrument Science Report, ACS 2011-03, (Baltimore:STScI) (ISR-III)
- Bohlin, R. C., et al. 2005, Instrument Science Report, ACS 2005-12, (Baltimore:STScI)
- Bohlin, R. C., et al. 2011, AJ, 141, 173
- De Marchi, G., Sirianni, M., Gilliland, R., Bohlin, R., Pavlovsky, C., Jee, M., Mack, J., van der Marel, R., & Boffi, F. 2004, Instrument Science Report, ACS 2004-08, (Baltimore:STScI) (DeM)
- Gilliland, R. L. 2004, Instrument Science Report, ACS 2004-01, (Baltimore:STScI)
- Gilliland, R. L., Bohlin, R. C., & Mack, J. 2006, Instrument Science Report, ACS 2006-06, (Baltimore:STScI)
- Gilliland, R. L., & Bohlin, R. C. 2007, Instrument Science Report, ACS 2007-01, (Baltimore:STScI)
- Goudfrooij, P., Wolfe, M. A., Bohlin, R. C., Proffitt, C. R., & Lennon, D. J. 2009, Instrument Science Report, STIS 2009-02, (Baltimore:STScI)
- Mack, J., Bohlin, R., Gilliland, R., Van der Marel, R., Blakeslee, J., & DeMarchi, G. 2002, Instrument Science Report, ACS 02-08, (Baltimore:STScI)
- Mack, J., Gilliland, R. L., Anderson, J., & Sirianni, M. 2007, Instrument Science Report, ACS 2007-02, (Baltimore:STScI)
- Sirianni, M., et al. 2005, PASP, 117, 1049S (S05)
- Smith, J. A., et al. 2002, AJ, 123,2121